NANO LETTERS

Letter

pubs.acs.org/NanoLett

Electrical Switch to the Resonant Magneto-Phonon Effect in Graphene

Przemyslaw Leszczynski,[†] Zheng Han,[‡] Aurelien A. L. Nicolet,[†] Benjamin A. Piot,[†] Piotr Kossacki,[§] Milan Orlita,[†] Vincent Bouchiat,[‡] Denis M. Basko,[∥] Marek Potemski,[†] and Clement Faugeras*[,†]

[†]LNCMI (CNRS, UJF, UPS, INSA), BP 166, 38042 Grenoble Cedex 9, France

[‡]Institut Néel, CNRS-UJF-INP, 38042 Grenoble Cedex 09, France

[§]Institute of Experimental Physics, University of Warsaw, Hoza 69, Warsaw 00-681, Poland

[∥]Université Grenoble 1/CNRS, LPMMC UMR 5493, 25 rue des Martyrs, 38042 Grenoble, France

Supporting Information

ABSTRACT: We report a comprehensive study of the tuning with electric fields of the resonant magneto-exciton optical phonon coupling in gated graphene. For magnetic fields around $B \sim 25$ T that correspond to the range of the fundamental magneto-phonon resonance, the electron−phonon coupling can be switched on and off by tuning the position of the Fermi level in order to Pauli block the two fundamental inter-Landau level excitations. The effects of such a profound change in the electronic excitation spectrum are traced through investigations of the optical phonon response in polarization resolved magneto-Raman scattering experiments. We report on the observation of a splitting of the phonon feature with satellite peaks developing at particular values of the Landau level filling factor on the low or on the high energy side of the phonon, depending on the relative energy of the discrete electronic excitation and of the optical phonon. Shifts of the phonon energy as large as ±60 cm^{-1} are observed close to the resonance. The intraband electronic excitation, the cyclotron resonance, is shown to play a relevant role in the observed spectral evolution of the phonon response.

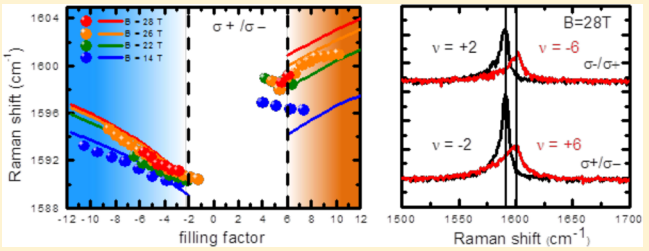

KEYWORDS: *Graphene, Raman spectroscopy, magneto-phonon resonance, electron−phonon interaction*

In graphene, optical phonons from the Brillouin zone center effectively couple to electronic excitations with the total momentum $\mathbf{k} = 0$. This coupling may lead to absorption of phonons by electrons, which manifests itself as a broadening of the G peak in the Raman spectrum. Similar $\mathbf{k} = 0$ electronic excitations determine the absorption of electromagnetic radiation, proportional to the dissipative optical conductivity. Despite the difference between the two families of electronic excitations (phonons couple to valley-antisymmetric excitations, while the optical conductivity is determined by valley-symmetric excitations[1]) in many situations their spectra can be assumed to be the same (unless some strong intervalley scattering processes are present). The low energy excitation spectra of graphene can be modified by external means, for instance, by tuning the position of the Fermi level with an electrostatic gate[2] or by applying an intense magnetic field perpendicular to the plane of the graphene crystal.[3,4] The electron−phonon interaction in graphene is particularly efficient for such optical-like electronic excitations and, as a result, the effects related to the electron−phonon interaction in graphene can be tuned externally by modifying the electronic excitation spectrum. Graphene hosts two Kohn anomalies at the Γ and K points of the Brillouin zone.[5] The energies of optical phonons at these two specific points are affected by the electron−phonon interaction at the level of 2−4%. As a result, the phonon energy as well as its line width, as seen through a Raman scattering experiment, can be tuned externally by modifying the electronic excitation spectrum, for instance, by changing the position of the Fermi level,[6,7] or by applying a strong magnetic field.[1,8]

An applied magnetic field (B) induces Landau quantization and changes the continuous interband electronic excitation spectrum at $B = 0$ into a discrete excitation spectrum between highly degenerated Landau levels of index n with an energy that increases with the magnetic field as $E_n = \mathrm{sign}(n)(2|n|)^{1/2}(\hbar v_F/l_B)$, where v_F is the Fermi velocity and $l_B = 1/(e|B|/\hbar)^{1/2}$ is the magnetic length. The electronic excitations $L_{n,m}$ between Landau levels of indices n and m, relevant for the electron−phonon interaction are those fulfilling the optical selection rule $|n| - |m| = \pm 1$. In the following, we will refer to these excitations as optical-like excitations. When these specific excitations are tuned to the phonon energy by increasing the strength of the magnetic field, the electron−phonon interaction becomes resonant, between one discrete inter Landau level

Received: December 11, 2013
Revised: January 29, 2014
Published: February 3, 2014

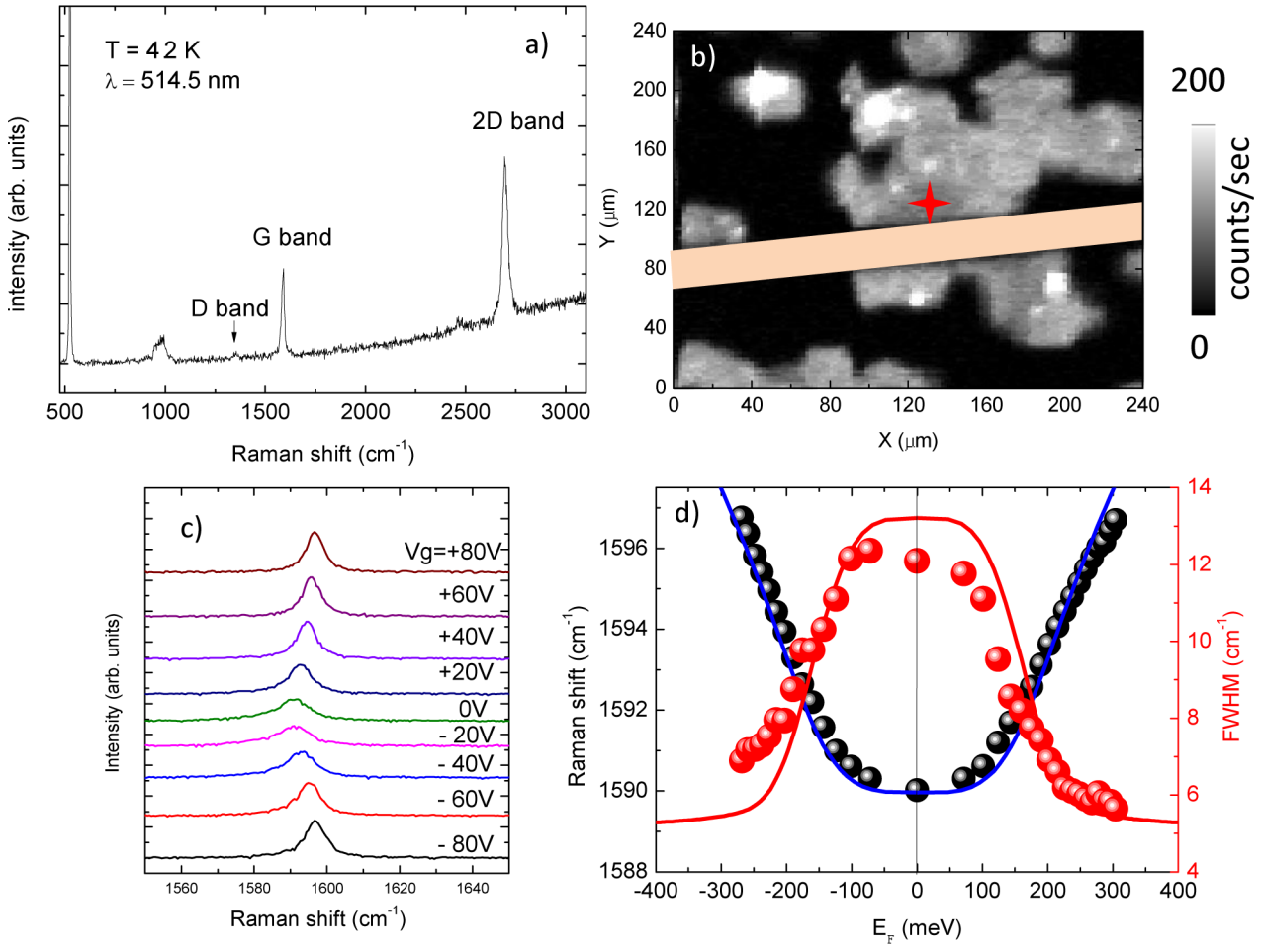

Figure 1. (a) Typical Raman scattering spectrum of the sample measured at temperature 4.2 K with a 514.5 nm excitation. (b) Grayscale map of the G band feature intensity. The metallic gate electrode is drawn in the middle of the flake and the red star is the location at which measurements have been performed. (c) Typical spectra at $B = 0$ T for different values of the gate voltage. (d) Evolution of the phonon energy (black points) and fwhm (red points) as a function of the Fermi level. The blue (red) line is the calculated evolution of the phonon energy (fwhm) according to the model described in the text. A Gaussian-type distribution of carrier density with a standard deviation of $\sigma = 1.27 \times 10^{12}$ cm^{-2} has been used (see text).

electronic excitation and the phonon mode. This interaction manifests itself through the magneto-phonon resonance, a series of avoided crossings between the phonon mode and the electronic excitation spectrum each time a $\Delta|n| = \pm 1$ inter-Landau excitation is tuned to the phonon energy.[9−14] Magneto-phonon resonance has also been observed in multilayer graphene specimens[15] in bulk graphite for both H and K point carriers[16,17] and is now a tool to study the electron−phonon interaction and to perform the Landau level spectroscopy of unknown systems. At the resonance, the splitting energy depends on the effective oscillator strength of the electronic excitation which is determined by the strength of the magnetic field and by the occupancy of the initial and final Landau levels implied in the excitation. Up to now, most magneto-Raman scattering experiments have been performed on graphene specimens with a fixed carrier density n_s.[13,14] Recently, Remi et al.[18] reported on unpolarized Raman scattering experiments on a gated graphene sample at $B = 12.6$ T in the nonresonant regime. Here, we demonstrate experimentally that, by changing the position of the Fermi level among the Landau levels with electrostatic gating, it is possible in graphene in a magnetic field, to externally switch on and off the resonant electron−phonon interaction.

For high enough magnetic fields ($B > 5$ T), all interband Landau level excitations have an energy higher than that of the optical phonon, except for the $L_{-1,0}$ and $L_{0,1}$ excitations, whose transition frequency $T_0 = \sqrt{2}v_F/l_B$ matches that of the phonon at $B \sim 25$ T. The $L_{0,1}$ and $L_{-1,0}$ excitations, active in distinct crossed circular polarization configurations, when activated by adjusting the filling factor $\nu = hn_s/(eB)$ between $\nu = +6$ and $\nu = -6$ profoundly affect the phonon energy through their resonant coupling to the phonon mode. This effect, together with the coupling to the intraband cyclotron resonance mode, can be traced by performing polarization resolved magneto-Raman scattering experiments for different values of the Fermi energy, the results of which are described in this paper.

Experimental Procedure. Graphene single grains on Cu were grown by chemical vapor deposition (CVD). During the growth, temperature was kept at 1000 °C, while partial pressures for hydrogen and methane were 25 and 50 μbar, respectively. The growth was stopped at 5 min, before graphene grains merge into a continuous layer. The graphene grains were then transferred onto 285 nm SiO_2/Si wafer with the PMMA-assisted method.[19] Those randomly scattered graphene grains on SiO_2 were finally contacted with arrays of long metallic leads (50 nm Au/5 nm Ti), each lead serving as an individual ground. When patterned into a Hall bar geometry, such samples show a

dx.doi.org/10.1021/nl404588g | Nano Lett. 2014, 14, 1460−1466

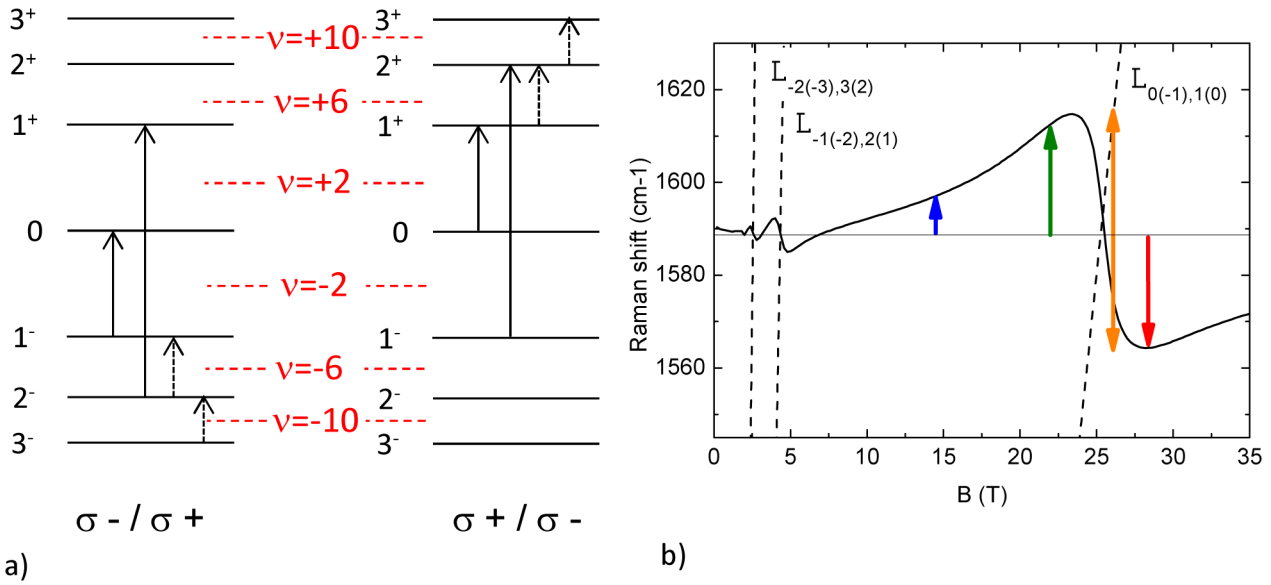

Figure 2. (a) Schematic of the Landau level structure in graphene at finite magnetic field with relevant interband (solid arrows) and intraband (dotted arrows) excitations in both polarization configuration. (b) Calculated evolution of the G band energy for neutral graphene as a function of the magnetic field for $\sigma+/\sigma-$ configuration. Dashed lines represent $\Delta|n| = \pm 1$ electronic excitations that couple to the phonon and colored arrows indicate the magnetic fields at which the filling factor has been experimentally varied. The length of the arrow indicates the magnitude of the expected energy shift. The horizontal solid line indicates the $B = 0$ phonon energy.

typical electronic mobility of ~4000 $cm^2 \cdot (V \cdot s)^{-1}$. Polarization-resolved Raman scattering measurements have been performed with a homemade miniaturized optical bench[11] based on optical fibers, lenses and band-pass filters. The excitation laser at λ = 514.5 nm is delivered through a monomode optical fiber of ~5 μm core, the scattered light is collected with a 50 μm optical fiber and analyzed by a 50 cm grating spectrometer equipped with a nitrogen cooled charge-coupled device (CCD) camera. The excitation power was set to 4 mW focused on an ~1 μm diameter spot. This system allows for the measurement of the Raman scattering response of graphene at liquid helium temperature and in magnetic fields up to 30 T. We have used the crossed circular polarization configurations $\sigma\pm/\sigma\mp$ (excitation light polarization/collection light polarization), which select $\Delta|n| = \pm 1$ electronic excitations and optical phonons at the Γ point (G band)[16,20] in graphene. Measurements have been performed either at a fixed gate voltage while sweeping the magnetic field, or at constant magnetic field while sweeping the gate voltage.

Figure 1a shows a typical Raman scattering spectrum of the graphene flake that has been investigated in magnetic fields. The 2D band has a single Lorentzian shape, characteristic of a graphene monolayer.[21] Figure 1b shows a spatial map of the G band intensity and helps to visualize the shape of the flake together with the electrode. The bright spots appearing in this figure correspond to bilayer graphene with a non Bernal stacking, which are typical of CVD grown graphene. They are characterized by a G band intensity 30 times enhanced in our sample with respect to the G band feature at nearby locations, by a single Lorentzian-shaped 2D band feature slightly blue-shifted and by an additional feature, the R band, observed in the present case at 1490 cm^{-1} [17,22,23] (see Supporting Information). Measurements were performed at the location indicated by the red star in Figure 1 b), close to the electrode.

Tuning the position of the Fermi energy at low temperature leads to a renormalization of the phonon energy and of its full width at half-maximum (fwhm)[6,7] as a result of the changes of the density of states at the Fermi energy and of the gradual quenching of low energy electronic excitations due to Pauli blocking. Typical Raman scattering spectra for different values of the gate voltage are presented in Figure 1c. The evolution of the phonon energy and fwhm as a function of the Fermi energy, obtained experimentally, is shown in Figure 1d together with the result of the theoretical modeling of this effect.[24] In the modeling, we used the value ω_0 = 1588.7 cm^{-1} for the phonon frequency of the undoped sample at zero magnetic field, the dimensionless electron−phonon coupling constant $\lambda = 4.0 \times 10^{-3}$, and the Fermi velocity $\nu_F = 1.08 \times 10^6$ m/s. The electronic transitions are assumed to be homogeneously broadened with the broadening parameter $\hbar\gamma$ = 12 meV. In addition, the inhomogeneous spatial fluctuations of the electronic density are accounted for by a convolution of the results obtained at a fixed density with the Gaussian distribution of densities, characterized by a standard deviation of $\sigma = 1.27 \times 10^{12}$ cm^{-2}. The Fermi velocity is determined by the observation of the resonant coupling of the $L_{0,1}$ inter-Landau level excitation with the optical phonon at $B \sim 25$ T (see Supporting Information). The Fermi energy E_F was deduced from the applied gate voltage V_g using the relation $n_s = \alpha V_g$ where $\alpha = 7.56 \times 10^{10}$ cm^{-2} V^{-1} for a 285 nm thick SiO_2 layer and $E_F = \hbar\nu_F(\pi n_s)^{1/2}$. A hysteresis in the position of the Dirac point was observed between consecutive gate voltage sweeps and shifts ΔV_{Dirac} up to ±8 V have been corrected.

Theoretical Modeling of the Raman Spectrum. The Raman spectrum is assumed to be proportional to the phonon spectral function $-(1/\pi)\mathrm{Im}D_\pm(\omega)$, determined by the retarded phonon propagator,

$$D_\pm(\omega) = \frac{2\omega_0}{\omega^2 - \omega_0^2 - 2\lambda\omega_0\Pi_\pm(\omega)} \quad (1)$$

Here $\Pi_\pm(\omega)$ is the retarded polarization operator which is diagonal in the circular basis, the two circular polarizations being denoted by ±. The polarization operator can be

dx.doi.org/10.1021/nl404588g | Nano Lett. 2014, 14, 1460−1466

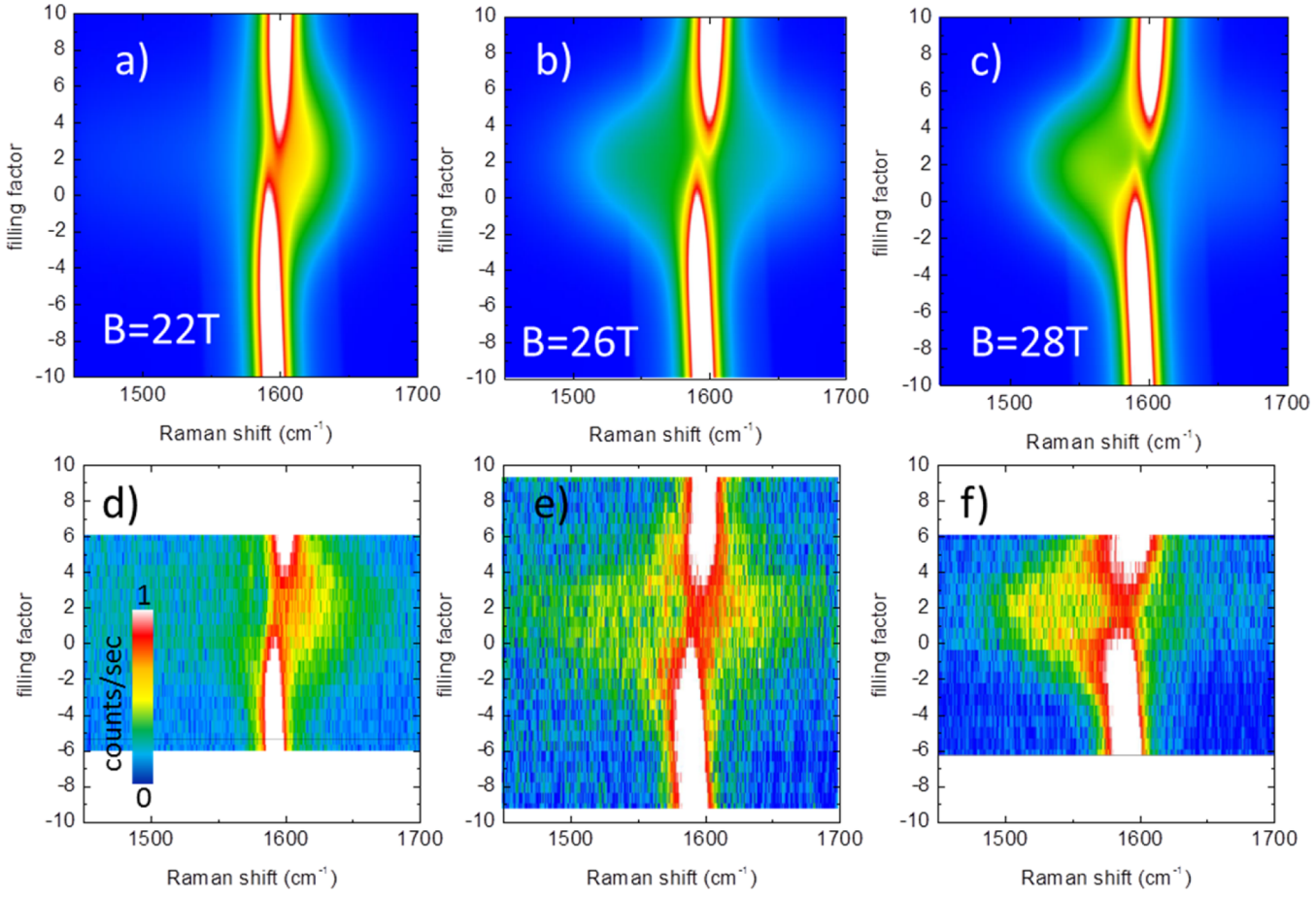

Figure 3. (a–c) False color map of the calculated phonon spectral function in the $\sigma+/\sigma-$ polarization configuration as a function of the filling factor for B = 22, 26, and 28 T, respectively, and with a Gaussian-type distribution of carrier density with a standard deviation of 1.27×10^{12} cm^{-2}. (d–f) False color map of the experimental results in the same range of filling factors at B = 22, 26, and 28 T, respectively. The color scale has been arranged in order to see the satellite peaks. The main phonon feature is seen with a yield of 3.5 counts/sec.

straightforwardly evaluated, at an arbitrary filling factor ν, following the procedure described in refs 1 and 8. Keeping all the nonresonant terms (some of which were omitted in refs 1 and 8), we obtain

$$\Pi_{\pm}(\omega) = \sum_{n=n_F}^{\infty} \frac{\frac{\omega(\omega+i\gamma)T_0^2}{T_n}}{(\omega+i\gamma)^2 - T_n^2} + \sum_{n=0}^{n_F-1} \frac{T_0^2}{T_n} + W_\nu \tag{2}$$

$$W_{\nu>2} = \frac{T_0^2}{2}\left(\frac{f}{T_{n_F}} - \frac{1-f}{T_{n_F-1}} - \frac{1-f}{\omega_c^-} - \frac{f}{\omega_c^+}\right) + \frac{\omega T_0^2}{2}\left[-\frac{\frac{f}{T_{n_F}}}{\omega+i\gamma\pm T_{n_F}} + \frac{\frac{(1-f)}{T_{n_F-1}}}{\omega+i\gamma\mp T_{n_F-1}}\right] + \frac{\omega T_0^2}{2}\left[\frac{\frac{(1-f)}{\omega_c^-}}{\omega+i\gamma\mp\omega_c^-} + \frac{\frac{f}{\omega_c^+}}{\omega+i\gamma\mp\omega_c^+}\right] \tag{3}$$

$$W_{-2<\nu<2} = \pm\frac{\omega T_0^2(2f-1)}{(\omega+i\gamma)^2 - T_0^2} \tag{4}$$

$$W_{\nu<-2} = \frac{T_0^2}{2}\left(\frac{1-f}{T_{n_F}} - \frac{f}{T_{n_F-1}} - \frac{f}{\omega_c^-} - \frac{1-f}{\omega_c^+}\right) + \frac{\omega T_0^2}{2}\left[-\frac{\frac{(1-f)}{T_{n_F}}}{\omega+i\gamma\mp T_{n_F}} + \frac{\frac{f}{T_{n_F-1}}}{\omega+i\gamma\pm T_{n_F-1}}\right] + \frac{\omega T_0^2}{2}\left[\frac{\frac{f}{\omega_c^-}}{\omega+i\gamma\pm\omega_c^-} + \frac{\frac{(1-f)}{\omega_c^+}}{\omega+i\gamma\pm\omega_c^+}\right] \tag{5}$$

Here we denoted by $n_F \geq 0$ the (non-negative) index of the Landau level which is partially filled (the integer part of $|\nu|/4 + 1/2$), and by f the average electronic occupation of this partially filled level ($0 \leq f < 1$). We also introduced the interband transition frequency $T_n = (n^{1/2} + (n+1)^{1/2})T_0$ and the two intraband frequencies corresponding to the cyclotron resonance, $\omega_c^+ = ((n_F+1)^{1/2} - (n_F)^{1/2})T_0$ and $\omega_c^- = ((n_F)^{1/2} - (n_F - 1)^{1/2})T_0$. The electronic damping γ is introduced phenomenologically, keeping in mind that $\Pi_{\pm}(\omega)$ should satisfy the general condition: $\mathrm{sign}(\mathrm{Im}\,\Pi_{\pm}(\omega)) = -\mathrm{sign}(\omega)$, and should be continuous upon the change of the filling factor when $n_F \to n_F + 1$.

Gate Dependence Close to the Resonant Condition. Figure 2a shows a schematic of the 4-fold degenerate Landau

dx.doi.org/10.1021/nl404588g | Nano Lett. 2014, 14, 1460–1466

levels in graphene with an applied magnetic field together with the interband (solid arrows) and intraband (dashed arrows) excitations that are allowed in the two crossed circular configurations $\sigma\pm/\sigma\mp$ and that can be probed selectively with polarization resolved Raman scattering techniques. Depending on the value of the filling factor, both intraband and interband excitations can be active or quenched due to Pauli blocking. For instance, the $L_{0,1}$ excitation is allowed for $-2 < \nu < +6$ and its effective oscillator strength has the maximum at $\nu = +2$, while the $L_{-1,0}$ excitation is allowed for $-6 < \nu < +2$ and its effective oscillator strength is the largest at $\nu = -2$. Intraband excitations are only active in the $\sigma-/\sigma+$ configuration for $\nu > +2$ and in the $\sigma+/\sigma-$ configuration for $\nu < -2$. Similar conditions on the filling factor can be derived for these excitations and, for instance, the $L_{1,2}$ excitation is allowed for $+2 < \nu < +10$ and has a maximum effective oscillator strength at $\nu = +6$, when the first Landau level is completely occupied and the second Landau level is fully depleted. Figure 2b shows the evolution of the phonon energy for neutral graphene, which displays the pronounced oscillations representative of the magneto-phonon resonance, when the interband excitations are tuned, one after another, in resonance with the phonon energy. We have selected the values of the magnetic field, indicated by the colored arrows in this figure, at which we have measured the carrier density dependent magneto-Raman scattering response. At $B = 14$ T, the electron−phonon interaction is not resonant, but the observed phonon energy is sensitive to either the $L_{0,1}$ or the $L_{-1,0}$ excitations, which increase slightly the phonon energy with respect to its $B = 0$ energy, when they are active.[18] These two particular electronic excitations are tuned to the phonon energy at $B \sim 25$ T. Hence, $B = 22$, 26, and 28 T represent the different cases just below the resonance, on the resonance, and above the resonance, respectively. The expected changes in the phonon energy, when the $L_{0,1}$ or $L_{-1,0}$ excitations are turned on or off by adjusting the carrier density, are completely different in these three regimes: (i) below the resonance, the phonon energy is expected to increase when $L_{0,1}$ or $L_{-1,0}$ is turned on, (ii) close to the resonance, the phonon should split into two components in clean enough systems, one with an increased energy and the other one with a reduced energy, and finally (iii) above the resonance, the phonon energy is expected to decrease.

The results of such experiments performed in the $\sigma+/\sigma-$ configuration are shown in Figure 3d−f in the form of false color maps of the scattered intensity in the range of the optical phonon as a function of the filling factor for $B = 22$, 26, and 28 T, respectively. Figure 3a−c shows the result of the calculation of the spectral function as defined in eq 1 for the same values of the magnetic field as a function of the filling factor. As before, we have included inhomogeneous spatial fluctuations of the electronic density by doing a convolution of the results obtained at a fixed density with the Gaussian distribution of densities, characterized by a standard deviation of $\sigma = 1.27 \times 10^{12}$ cm $^{-2}$. The observed shift of the spectral weight of the phonon feature is representative of the magneto-phonon resonance with shifts of the phonon energy as large as ± 60 cm^{-1}. As shown in Figure 4b, the additional feature that appears when the $L_{0,1}$ excitation is active in the $\sigma+/\sigma-$ configuration has a fwhm as large as ~ 50 cm^{-1}, only exists when the filling factor is between $\nu = -2$ and $\nu = +6$ and the observed shift is maximum close to $\nu = +2$, when the effective oscillator strength of the $L_{0,1}$ excitation is maximum. If the carrier density were spatially homogeneous across the sample, a single component

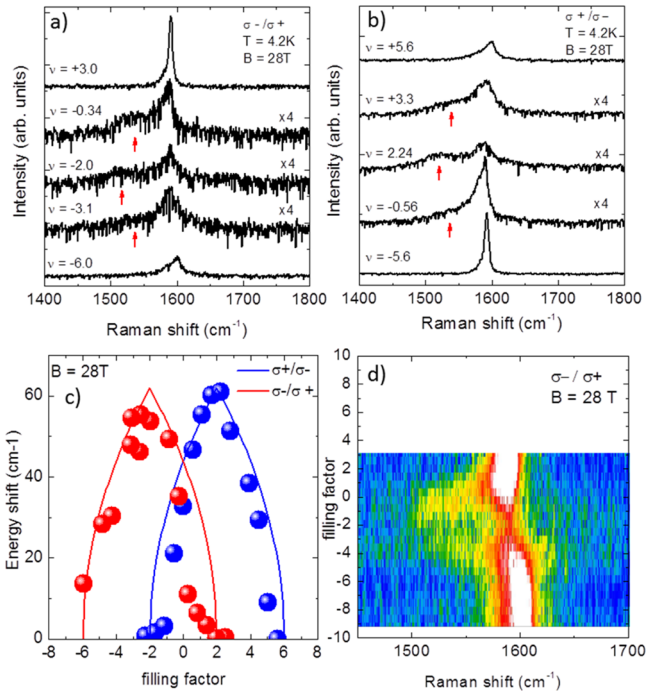

Figure 4. (a,b) Typical Raman scattering spectra measured at $B = 28$ T in the $\sigma-/\sigma+$ and in the $\sigma+/\sigma-$ polarization configuration respectively for different values of the filling factor. Red arrows indicate the position of the shifted phonon feature. (c) Evolution of the phonon splitting energy as a function of the filling factor in the $\sigma-/\sigma+$ (red dots) and $\sigma+/\sigma-$ (blue dots) together with the expected square-root dependence (solid lines). (d) False color map of the measured scattered intensity in the $\sigma-/\sigma+$ polarization configuration as a function of the filling factor at $B = 28$ T.

should be observed for all values of the filling factor (see Supporting Information). Spatial inhomogeneities of the carrier density at the nm-scale mix the Raman scattering response of graphene locations with different apparent strength of electron−phonon coupling. This leads to the observation of two phonon features even when $-2 < \nu < +6$. This behavior is reproduced in the calculations by taking into account such inhomogeneities (see Supporting Information).

As can be seen in Figure 4a,d, in the $\sigma-/\sigma+$ polarization configuration a pronounced shift of the phonon spectral weight is also observed but the amplitude of the splitting is now maximum at $\nu = -2$, when the effective oscillator strength of the $L_{-1,0}$ electronic excitation, active in this configuration, is maximum. These polarization resolved Raman scattering experiments unambiguously demonstrate the coupling of electronic excitations and optical phonons in graphene, both excitations having a similar angular momentum ± 1. At $B = 28$ T, we have determined the energy shift of the phonon feature that is presented in Figure 4c as a function of the filling factor, together with the expected square-root dependence (solid lines), as expected from ref 1. This energy difference represents half of the total energy split, because at $B = 28$ T only the low energy component of the coupled magneto-exciton−phonon mode is observed. The overall agreement between these data and existing theories is very good and such experiment offers a possibility to trigger the resonant electron−phonon interaction by electrical means and to gradually reach a strongly interacting regime.

dx.doi.org/10.1021/nl404588g | Nano Lett. 2014, 14, 1460−1466

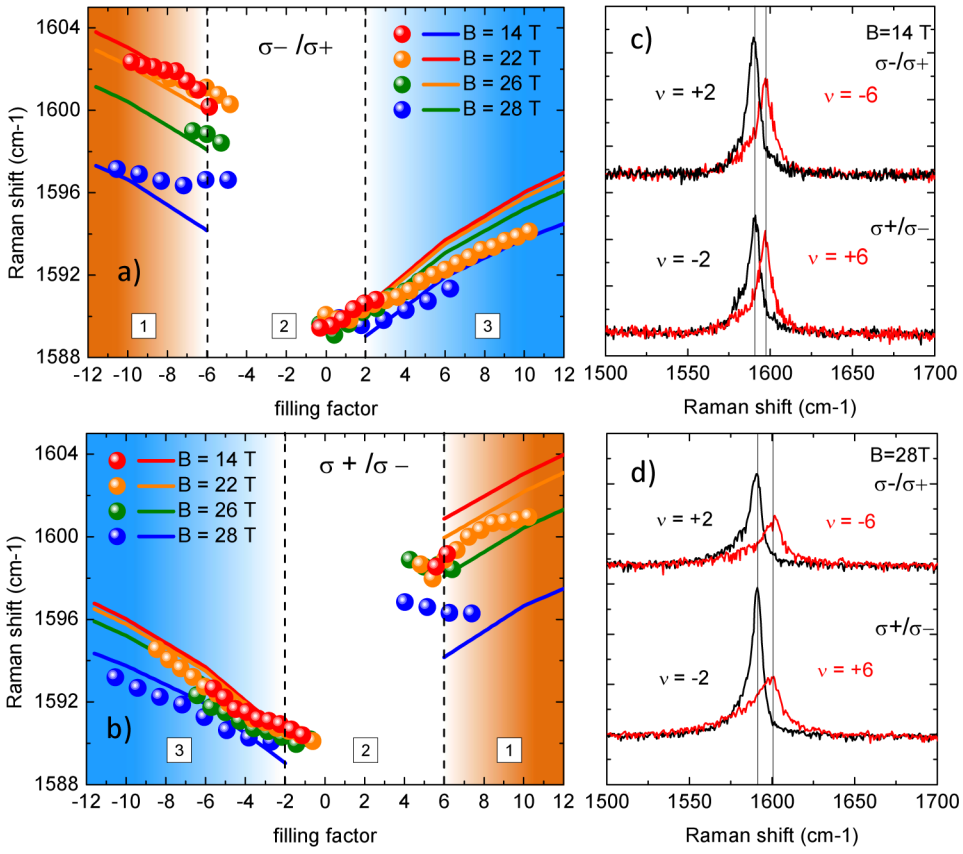

Figure 5. (a,b) Evolution of the phonon energy in the $\sigma-/\sigma+$ and $\sigma+/\sigma-$ configurations respectively, as a function of the filling factor for different values of the magnetic field (points) together with theoretical expectations including intraband excitations (solid lines). (c,d) Typical polarization resolved Raman scattering spectra for $\nu = +2$ and $\nu = -6$ at $B = 14$ T and $B = 28$ T.

Gate Dependence at High Filling Factor Values. When the filling factor is tuned to high values so that the $L_{0,1}$ or the $L_{-1,0}$ is turned off, the contribution of the electron phonon interaction to the phonon energy is determined by interband electronic excitations, involving Landau levels of high index, with an energy much higher than the phonon energy and by intraband excitations. Gradually quenching such interband excitations by increasing the Fermi energy (or the absolute value of the filling factor) leads to an increase of the phonon energy. In the range of magnetic fields addressed in this study, the intraband excitations have an energy much lower than the phonon energy (at $B = 26$ T, the frequencies of the $L_{1(-2),2(-1)}$ and $L_{2(-3),3(-2)}$ transitions are $T_1 = 670$ cm^{-1} and $T_2 = 510$ cm^{-1}, respectively) but they participate to the phonon renormalization by slightly increasing its energy. This effect is more pronounced as the magnetic field is increased, as it is shown in Figure 5a,b) in both polarization configurations. The solid lines in this figure represent the expected phonon energy at different values of the magnetic field, as a function of the filling factor. They were found by calculating the positions of the poles of $D_{\pm}(\omega)$ (eq 1) in the complex plane ω, using the parameters corresponding to the experimental conditions and presented in the preceding section. As can be seen in regions 3 of Figure 5a,b when the intraband excitation is not active (for $\nu > +2$ in $\sigma-/\sigma+$ configuration and for $\nu < -2$ in $\sigma+/\sigma-$ configuration), the theoretical expressions eq 1 describe quite well the experimentally determined phonon energies in terms of energy and of its evolution when increasing the filling factor. In the opposite range of filling factor, shown in parts 1 of Figure 5a,b, the effect of intraband excitations is clearly visible when comparing the spectra obtained at $\nu = +2$ and $\nu = -6$ in the $\sigma-/\sigma+$ configuration and spectra at $\nu = -2$ and $\nu = +6$ in the $\sigma+/\sigma-$ (see Figure 5c,d). Without considering intraband excitations, these spectra should be identical because they correspond to situations when only the fundamental interband excitation is quenched while higher energy excitations are allowed in both polarization configuration and have the same energy in the first approximation. The spectra presented in Figure 5c,d clearly show that the phonon energy measured at these particular values of the filling factor differ and that the energy shift increases with increasing magnetic fields. These experiments show however that there is a correspondence between spectra measured in the $\sigma-/\sigma+$ at $\nu = -6$ and those measured in the $\sigma+/\sigma-$ configuration at $\nu = +6$, which is a consequence of the electron−hole symmetry. In these two situations, the filling factor is such that the intraband excitation ($L_{-2,-1}$ or $L_{1,2}$) has a maximized and identical effective oscillator strength. The observed difference in the phonon energy measured at $\nu = \pm 2$ and at $\nu = \mp 6$ is a direct measurement of the coupling between the intraband electronic excitation (cyclotron resonance) and the optical phonon coupling, and is properly described by the expressions given in eqs 2−5.

Conclusion. We have shown that the resonant interaction between magneto-excitons and optical phonons in graphene can be switched on and off by controlling the position of the Fermi level, and hence, quenching or allowing the specific electronic excitations through Pauli blocking. We have explored the three regimes for which the electronic excitation lies below,

dx.doi.org/10.1021/nl404588g | *Nano Lett.* 2014, 14, 1460−1466

is degenerated with, or is above the optical phonon mode. These three regimes have distinct signatures when monitoring the position of the Fermi level. In the resonant regime, satellite peaks appear when the $L_{0(-1),1(0)}$ excitation is active and energy shifts of the phonon feature up to 60 cm^{-1} has been observed that evolves with v as expected theoretically. Experimental results in the resonant regime, together with the effect of cyclotron resonance are well reproduced by existing theories. Such experiments offer a new insight into the electron−phonon interaction in graphene by offering the possibility to continuously tune the electron−phonon system from weakly to strongly interacting regime, and they could be extended to multilayer graphene systems or to hybrid graphene/2D materials heterostructures.

■ ASSOCIATED CONTENT

Supporting Information

Twisted bilayer inclusions characterization, determination of the Fermi velocity, effect of a carrier density distribution on the observed Raman scattering spectra, and additional data measured on a different sample. This material is available free of charge via the Internet at http://pubs.acs.org.

■ AUTHOR INFORMATION

Corresponding Author

*E-mail: clement.faugeras@lncmi.cnrs.fr.

Notes

The authors declare no competing financial interest.

■ ACKNOWLEDGMENTS

Part of this work has been supported by the graphene flagship project, and by the European Research Council (ERC-2012-AdG-320590-MOMB)

■ REFERENCES

(1) Goerbig, M. O.; Fuchs, J.-N.; Kechedzhi, K.; Fal'ko, V. I. *Phys. Rev. Lett.* **2007**, *99*, 087402.
(2) Li, Z.; Henriksen, E.; Jiang, Z.; Hao, Z.; M.C. Martin a, d. P. K.; Stormer, H.; Basov, D. *Nat. Phys.* **2009**, *4*, 532.
(3) Sadowski, M. L.; Martinez, G.; Potemski, M.; Berger, C.; de Heer, W. A. *Phys. Rev. Lett.* **2006**, *97*, 266405.
(4) Jiang, Z.; Henriksen, E. A.; Tung, L. C.; Wang, Y.-J.; Schwartz, M. E.; Han, M. Y.; Kim, P.; Stormer, H. L. *Phys. Rev. Lett.* **2007**, *98*, 197403.
(5) Piscanec, S.; Lazzeri, M.; Mauri, F.; Ferrari, A. C.; Robertson, J. *Phys. Rev. Lett.* **2004**, *93*, 185503.
(6) Pisana, S.; Lazzeri, M.; Casiraghi, C.; Novoselov, K. S.; Geim, A. K.; Ferrari, A. C.; Mauri, F. *Nat. Mater.* **2007**, *6*, 198.
(7) Yan, J.; Zhang, Y.; Kim, P.; Pinczuk, A. *Phys. Rev. Lett.* **2007**, *98*, 166802.
(8) Ando, T. *J. Phys. Soc. Jpn.* **2007**, *76*, 024712.
(9) Faugeras, C.; Amado, M.; Kossacki, P.; Orlita, M.; Sprinkle, M.; Berger, C.; de Heer, W. A.; Potemski, M. *Phys. Rev. Lett.* **2009**, *103*, 186803.
(10) Yan, J.; Goler, S.; Rhone, T. D.; Han, M.; He, R.; Kim, P.; Pellegrini, V.; Pinczuk, A. *Phys. Rev. Lett.* **2010**, *105*, 227401.
(11) Faugeras, C.; Amado, M.; Kossacki, P.; Orlita, M.; Kühne, M.; Nicolet, A. A. L.; Latyshev, Y. I.; Potemski, M. *Phys. Rev. Lett.* **2011**, *107*, 036807.
(12) Kühne, M.; Faugeras, C.; Kossacki, P.; Nicolet, A. A. L.; Orlita, M.; Latyshev, Y. I.; Potemski, M. *Phys. Rev. B* **2012**, *85*, 195406.
(13) Kossacki, P.; Faugeras, C.; Kühne, M.; Orlita, M.; Mahmood, A.; Dujardin, E.; Nair, R. R.; Geim, A. K.; Potemski, M. *Phys. Rev. B* **2012**, *86*, 205431.
(14) Kim, Y.; Poumirol, J. M.; Lombardo, A.; Kalugin, N. G.; Georgiou, T.; Kim, Y. J.; Novoselov, K. S.; Ferrari, A. C.; Kono, J.; Kashuba, O.; Fal'ko, V. I.; Smirnov, D. *Phys. Rev. Lett.* **2013**, *110*, 227402.
(15) Faugeras, C.; Kossacki, P.; Nicolet, A.; Orlita, M.; Potemski, M.; Basko, D. *New J. Phys.* **2012**, *14*, 095007.
(16) Kossacki, P.; Faugeras, C.; Kühne, M.; Orlita, M.; Nicolet, A. A. L.; Schneider, J. M.; Basko, D. M.; Latyshev, Y. I.; Potemski, M. *Phys. Rev. B* **2011**, *84*, 235138.
(17) Kim, Y.; Ma, Y.; Imambekov, A.; Kalugin, N. G.; Lombardo, A.; Ferrari, A. C.; Kono, J.; Smirnov, D. *Phys. Rev. B* **2012**, *85*, 121403.
(18) Remi, S.; Goldberg, B. B.; Swan, A. K. 2013, arXiv:cond−mat/1307.6067.
(19) Li, X.; Cai, W.; An, J.; Kim, S.; Nah, J.; Yang, D.; Piner, R.; Velamakanni, A.; Jung, I.; Tutuc, E.; Banerjee, S. K.; Colombo, L.; Ruoff, R. S. *Science* **2009**, *324*, 1312−1314.
(20) Kashuba, O.; Fal'ko, V. I. *Phys. Rev. B* **2009**, *80*, 241404.
(21) Ferrari, A. C.; Basko, D. M. *Nat. Nanotechnol.* **2013**, *8*, 235−246.
(22) Carozo, V.; Almeidad, C.; Ferreira, E.; Cancado, L.; Achete, C.; Jorio, A. *Nano Lett.* **2011**, *11*, 4527.
(23) He, R.; Chung, T.-F.; Delaney, C.; Keiser, C.; Jauregui, L. A.; Shand, P. M.; Chancey, C. C.; Wang, Y.; Bao, J.; Chen, Y. P. *Nano Lett.* **2013**, *13*, 3594−3601.
(24) Ando, T. *J. Phys. Soc. Jpn.* **2006**, *75*, 124701.